INTERNATIONAL JOURNAL FOR NUMERICAL METHODS IN FLUIDS
Int. J. Numer. Meth. Fluids **29**: 935–950 (1999)

NUMERICAL INVESTIGATION OF A LAMINAR PULSATING FLOW IN A RECTANGULAR DUCT

A. YAKHOT*, M. ARAD AND G. BEN-DOR

Pearlstone Center for Aeronautical Engineering Studies, Department of Mechanical Engineering, Ben-Gurion University of the Negev, Beersheva 84105, Israel

SUMMARY

A pulsating laminar flow of a viscous, incompressible liquid in a rectangular duct has been studied. The motion is induced under an imposed pulsating pressure difference. The problem is solved numerically. Different flow regimes are characterized by a non-dimensional parameter based on the frequency (ω) of the imposed pressure gradient oscillations and the width of the duct (h). This, in fact, is the Reynolds number of the problem at hand. The induced velocity has a phase lag (shift) with respect to the imposed pressure oscillations, which varies from zero at very slow oscillations, to 90° at fast oscillations. The influence of the aspect ratio of the rectangular duct and the pulsating pressure gradient frequency on the phase lag, the amplitude of the induced oscillating velocity, and the wall shear were analyzed.

KEY WORDS: pulsating flow; high-order-accurate discretization

1. INTRODUCTION

The study of unsteady pulsating flows is of practical engineering importance. High speed (turbulent) pulsating flows occur in turbomachinery, rotor blade aerodynamics, reciprocating piston-driven flows, etc. Numerous experimental investigations were focused on fundamental studies of fully developed periodic pipe flows with sinusoidally varying pressure gradients (or flow rates). Low speed (laminar) pulsating flows were studied in order to analyze the flows through small pipes or in the blood circulation systems. Laminar flows are relatively simple for analytical (or numerical) analysis and are a natural choice to provide basic studies of fundamental hydrodynamic effects in pulsating flows.

An incompressible viscous fluid, which is forced to move under a pulsating pressure difference in a duct, has a number of characteristic properties. Some features of such a flow are similar to those occurring in the boundary layer on a body performing reciprocating harmonic oscillations. This is an extension of the problem of the boundary layer when a viscous fluid is bounded by an infinite plane surface that executes a simple harmonic oscillation, with frequency ω, in its own plane. The latter is the classic problem of the flow near an oscillating flat plate, which was first studied by Stokes [1]. For this type of flow, transverse waves occur in a viscous fluid, with the velocity perpendicular to the direction of propagation. Stokes introduced a new length scale, the depth of penetration of the viscous wave, $\delta = (2\nu/\omega)^{1/2}$. The

* Correspondence to: Pearlstone Center for Aeronautical Engineering Studies, Department of Mechanical Engineering, Ben-Gurion University of the Negev, Beersheva 84105, Israel.

CCC 0271–2091/99/080935–16$17.50

Received February 1997
Revised January 1998

amplitude of the transverse waves is rapidly damped by the factor $\exp(-y/\delta)$ as one moves away from the solid surface whose oscillations generate the waves. In addition, an oscillating fluid layer has a phase lag, $\phi = y/\delta$, with respect to the motion of the wall, which depends on a distance y, from the wall.

In the present study, the authors consider a pulsating laminar flow of a viscous, incompressible liquid in a rectangular duct. The influence of the duct aspect ratio, the imposed frequency and the amplitude on the phase lag and the amplitude of the induced oscillating flow are analyzed.

2. PULSATING FLOW THROUGH A DUCT

Considered is an incompressible liquid, forced under a pulsating pressure difference, to move in a rectangular duct of constant cross-sectional shape: $0 \le x \le a$, $0 \le y \le h$. A schematic drawing of the duct is presented in Figure 1. It is supposed that the motion is in the z-direction only, so that the velocity vector is $\mathbf{V} = [0, 0, u(x, y, t)]$. This means that the velocity is solely axial, and hence, the flow is fully developed. The governing equation is

$$\frac{\partial u}{\partial t} = \nu \nabla^2 u - \frac{1}{\rho}\frac{\partial p}{\partial z}, \quad \frac{\partial p}{\partial z} = -\frac{\gamma_p}{L}\sin(\omega t), \quad u|_\Gamma = 0, \tag{1}$$

where ∇^2 is the two-dimensional Laplacian operator and Γ denotes the boundary of the duct. It is convenient to use complex notation. Introducing a velocity function $f(x, y, t) = u(x, y, t) + iv(x, y, t)$, Equation (1) is rewritten in the following form:

$$\frac{\partial f}{\partial t} = \nu \nabla^2 f + \frac{i\gamma_p}{\rho L}\,\mathrm{e}^{-i\omega t}, \quad f|_\Gamma = 0, \tag{2}$$

when the velocity is the real part of the function $f(x, y, t)$ i.e., $u(x, y, t) = \mathscr{R}eal[f(x, y, t)]$. In Equation (2), γ_p and ω are the amplitude and the frequency of the pressure difference oscillations respectively. First, a one-dimensional case of a flow between two parallel plates ($0 \le y \le h$), which yields a simple solution in a closed form, is considered, *viz*.

$$f(y, t) = \frac{\gamma_p}{\rho L \omega}\,\mathrm{e}^{-i\omega t}\left[\frac{\cos k(y - h/2)}{\cos(kh/2)} - 1\right], \quad k = (1 + i)\alpha, \quad \alpha = (\omega/2\nu)^{1/2}. \tag{3}$$

Separating the real part of the function $f(y, t)$ gives the velocity $u(y, t) = \mathscr{R}eal[f(y, t)]$ in the form

$$u(y, t) = A(y)\cos(\omega t) + B(y)\sin(\omega t), \tag{4}$$

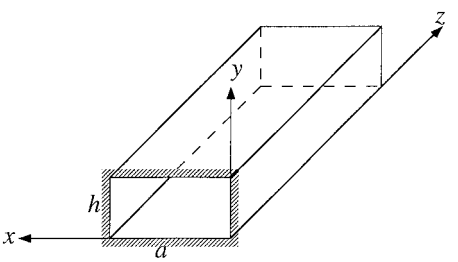

Figure 1. Schematic of a duct.

where

$$A(y) = \frac{\gamma_p}{\rho L \omega}\left[\frac{\cosh(\alpha y)\cos\alpha(h-y) + \cos(\alpha y)\cosh\alpha(h-y)}{\cosh(\alpha h) + \cos(\alpha h)} - 1\right] \tag{5}$$

and

$$B(y) = \frac{\gamma_p}{\rho L \omega}\frac{\sinh(\alpha y)\sin\alpha(h-y) + \sin(\alpha y)\sinh\alpha(h-y)}{\cosh(\alpha h) + \cos(\alpha h)}. \tag{6}$$

The solution given by Equation (4) can be rearranged by introducing the induced velocity amplitude γ_u, and the phase shift (lag) ϕ_u, with respect to the imposed pressure oscillations, *viz.*

$$u(y, t) = \gamma_u \sin(\omega t + \phi_u),$$

$$\gamma_u(y) = [A^2(y) + B^2(y)]^{1/2}, \qquad \tan\phi_u(y) = \frac{A(y)}{B(y)}, \tag{7}$$

where $A(y)$ and $B(y)$ are defined by Equations (5) and (6) respectively. Integrating the solution given by Equation (7) over the interval $0 \le y \le h$ results in the induced average velocity U_m

$$U_\mathrm{m} = \gamma_{U_\mathrm{m}} \sin(\omega t + \phi_{U_\mathrm{m}}), \tag{8}$$

Here γ_{U_m} and ϕ_{U_m} are the amplitude and the phase lag of the average velocity U_m. From Equation (7), the shear stress at the wall is

$$\tau_\mathrm{wall} = \mu \left.\frac{\partial u}{\partial y}\right|_{y=0} = \gamma_\tau \sin(\omega t + \phi_\tau). \tag{9}$$

In Equation (9), the relative amplitude of the wall shear stress $\gamma_\tau = \gamma_\tau(y)$, is introduced, and also its phase lag with respect to the imposed pressure oscillation, $\phi_\tau = \phi_\tau(y)$, which depend on the distance from the wall y. The expressions given by Equations (7)–(9) are the solution of the one-dimensional problem and these will be referred to in the following, when the features of a pulsating flow in a duct will be analyzed.

Substituting

$$f = \left(-\frac{\gamma_p}{\rho L \omega} + g\right) \mathrm{e}^{-i\omega t} \tag{10}$$

into Equation (2) gives the following for the function $g(x, y)$

$$\nabla^2 g + i\frac{\omega}{\nu} g = 0, \quad g|_\Gamma = \frac{\gamma_p}{\rho L \omega}. \tag{11}$$

As the next step, $g(x, y)$ is decomposed in terms of a pair of real-valued functions of the real variables x and y

$$g(x, y) = U(x, y) + iV(x, y). \tag{12}$$

After replacing $g(x, y)$ by Equation (12), the real and the imaginary parts of Equation (11) read

$$\nabla^2 U - \frac{\omega}{\nu} V = 0, \quad U|_\Gamma = \frac{\gamma_p}{\rho L \omega},$$

$$\nabla^2 V + \frac{\omega}{\nu} U = 0, \quad V|_\Gamma = 0. \tag{13}$$

The system of equations (13) has been solved numerically using a method based on a high-order-accurate discretization scheme, recently developed by Arad *et al.* [2,3]. The numerical method is discussed in the next section. From Equations (10) and (12), separating the real part of the function $f(x, y, t)$ yields, for the induced velocity $u(x, y, t)$,

$$u(x, y, t) = A(x, y)\cos(\omega t) + B(x, y)\sin(\omega t), \tag{14}$$

where

$$A(x, y) = U(x, y) - \frac{\gamma_p}{\rho L \omega}, \qquad B(x, y) = V(x, y). \tag{15}$$

The solution given by Equation (14) can be rearranged by introducing the amplitude γ_u, and the phase shift (lag) ϕ_u, with respect to the imposed pressure oscillations, *viz.*

$$u(x, y, t) = \gamma_u \sin(\omega t + \phi_u), \tag{16}$$

$$\gamma_u(x, y) = [A^2(x, y) + B^2(x, y)]^{1/2}, \qquad \tan\phi_u(x, y) = \frac{A(x, y)}{B(x, y)}, \tag{17}$$

where $A(x, y)$ and $B(x, y)$ are given by Equation (15). Integrating Equation (16) over the cross-section $0 \le x \le a$, $0 \le y \le h$ yields the induced cross-sectional mean velocity U_{m}, which also oscillates and can be expressed in the form given by Equation (8): $U_{\mathrm{m}} = \gamma_{U_{\mathrm{m}}} \sin(\omega t + \phi_{U_{\mathrm{m}}})$.

3. NUMERICAL METHOD

Equation(s) (13) are coupled Poisson equations. In 1941, Kantorovich and Krylov presented in a Russian edition of their book, the sixth-order accuracy nine-point discretization scheme for Poisson's equation. In 1964, the English edition of their book appeared [4]. Young and Dauwalder [5] studied numerous such high-order nine-point schemes in great details. For the general linear elliptic second-order partial differential equation, Young and Gregory [6] derived high-order discretization methods. They gave complete formulae and summarized the coefficients in a table for the high-order nine-point discretization scheme of a quite general type. For example, the sixth-order accuracy scheme, developed in Kantorovich and Krylov [4] for the Poisson equation, can be derived as a particular case from the general Young and Gregory scheme [6]. A considerable contribution in developing high-order-accurate finite difference discretization schemes for elliptic partial differential equations was done by Manohar and Stephenson [7–9]. The sixth-order nine-point discretization stencil for the Poisson equation with the Dirichlet boundary conditions on a rectangular domain was derived by Manohar and Stephenson [7].

The problem at hand is reduced to the system of equations (13), and its formulation is valid for a duct with an arbitrary cross-sectional shape. In this study, an *ad hoc* high-order-accurate discretization scheme, recently developed by Arad *et al.* [2,3], is applied for the system of equations (13), defined on a rectangular domain. The discrete equations for Equation(s) (13) on a nine-point discretization stencil are written in the form

$$aU_{i,j} + bS_{i,j}^{U(xy)} + cS_{i,j}^{U(x)} + dS_{i,j}^{U(y)} = r_U, \tag{18a}$$

$$aV_{i,j} + bS_{i,j}^{V(xy)} + cS_{i,j}^{V(x)} + dS_{i,j}^{V(y)} = r_V, \tag{18b}$$

where

$$S^{g(xy)}_{i,j} = g_{i-1,j-1} + g_{i-1,j+1} + g_{i+1,j-1} + g_{i+1,j+1},$$
$$S^{g(x)}_{i,j} = g_{i-1,j} + g_{i+1,j}, \qquad S^{g(y)}_{i,j} = g_{i,j-1} + g_{i,j+1}. \tag{19}$$

Equations (13) are coupled Poisson equations and their discrete form, Equations (18a,b), on a nine-point discretization stencil was derived in [4] using a high-order-accurate discretization scheme developed by Arad *et al.* [3]. The coefficients a, b, c, d in Equations (18a,b) are defined by

$$a = -\frac{5}{3}\left(\frac{1}{h_x^2} + \frac{1}{h_y^2}\right), \qquad b = \frac{1}{12}\left(\frac{1}{h_x^2} + \frac{1}{h_y^2}\right), \qquad c = \frac{1}{h_x^2} - 2b, \qquad d = \frac{1}{h_y^2} - 2b. \tag{20}$$

The right-hand-side terms in Equations (18a,b) are defined by

$$r_U = r\left(-\frac{\omega^2}{\nu^2}U, \frac{\omega}{\nu}V\right), \qquad r_V = r\left(-\frac{\omega^2}{\nu^2}V, -\frac{\omega}{\nu}U\right), \tag{21}$$

where

$$r(f,g) = g_{i,j} + \frac{1}{4!}(h_x^2 + h_y^2)f_{i,j} + \frac{2}{6!}(h_x^4 D_x^4 + 4h_x^2 h_y^2 D_x^2 D_y^2 + h_y^4 D_y^4)g_{i,j}$$
$$+ \frac{1}{4!}(h_x^2 - h_y^2)(D_x^2 - D_y^2)g_{i,j} + \frac{3}{2\cdot 6!}(h_x^2 - h_y^2)^2 D_x^2 D_y^2 g_{i,j}. \tag{22}$$

For $h_x = h_y = h$, the discretization coefficients reduce to

$$a = -\frac{10}{3h^2}, \qquad b = \frac{1}{6h^2}, \qquad c = d = \frac{2}{3h^2},$$
$$r(f,g) = g_{i,j} + \frac{2h^2}{4!}f_{i,j} + \frac{2h^4}{6!}(D_x^4 + 4D_x^2 D_y^2 + D_y^4)g_{i,j},$$

as has already been shown in [1,5,7].

The truncation error for the suggested scheme is of the sixth-order $O(h^6)$ on a square mesh ($h_x = h_y = h$) and of the fourth-order $O(h_x^4, h_x^2 h_y^2, h_y^4)$ on an unequally spaced mesh. The derivatives in Equation (22) should be calculated numerically. Here, an effective procedure is suggested, using the nine-point stencil, to compute them with the same high-order accuracy as the discretization scheme. It is readily seen from the discretization nine-point stencil definition, Equation(s) (19), that the mixed derivative could be computed using stencil's node values

$$D_x^2 D_y^2 g_{i,j} = \frac{1}{h_x^2 h_y^2}(S^{g(xy)}_{i,j} - 2S^{g(x)}_{i,j} - 2S^{g(y)}_{i,j} + 4g_{i,j}) + O(h_x^2, h_y^2). \tag{23}$$

Also, we have

$$D_x^2 g_{i,j} = \frac{1}{h_x^2}(S^{g(x)}_{i,j} - 2g_{i,j}) + O(h_x^2),$$
$$D_y^2 g_{i,j} = \frac{1}{h_y^2}(S^{g(y)}_{i,j} - 2g_{i,j}) + O(h_y^2). \tag{24}$$

The second-order accuracy in Equation (24) is enough because $(D_x^2 - D_y^2)$ is multiplied by $(h_x^2 - h_y^2)$ in Equation (22). That means that this term is evaluated only on an unequally spaced mesh when the scheme is of the fourth-order accuracy. The fourth-order derivatives in Equation (22) could be computed using the original equations (13)

$$D_x^4 g_{i,j} = D_x^2 f_{i,j} - D_x^2 D_y^2 g_{i,j},$$
$$D_y^4 g_{i,j} = D_y^2 f_{i,j} - D_x^2 D_y^2 g_{i,j}, \tag{25}$$

where

$$f_{i,j} = \begin{cases} \dfrac{\omega}{\nu} V_{ij} & \text{if } g_{i,j} = U_{ij} \\ -\dfrac{\omega}{\nu} U_{ij} & \text{if } g_{i,j} = V_{ij} \end{cases}.$$

Thus, one can see that computing the derivatives in Equation (22) with the aid of the expressions in Equations (23)–(25) gives for r_U and r_V the sixth-order accuracy $O(h^6)$ on a square mesh $(h_x = h_y = h)$ and the fourth-order accuracy $O(h_x^4, h_x^2 h_y^2, h_y^4)$ on an unequally spaced mesh.

To illustrate the high-order accuracy of the numerical scheme, the non-dimensional mean velocity amplitude, γ_{U_m}, is shown in Figure 2. The values of γ_{U_m} computed from Equation (16) are presented with successive computation meshes. The close-to-constant behavior of the high-order accuracy scheme results (solid lines) boldly illustrates the convergence, even on a coarse grid. On the other hand, it is seen that the results obtained on successive meshes with the standard second-order accuracy finite difference scheme (dashed lines) are different, and only the results on the finest grid could be considered as converged. The cases with $\alpha h \geq 10$ are more difficult for computations due to the oscillating behavior of the solution. In this case, the global error on a coarse mesh is high, while the results obtained with the suggested high-order scheme are practically converged. Figure 3 shows the ratio between the results obtained using the high-order (HO) and the standard finite difference (FD) schemes. Figure 4 presents the amplitude γ_u computed from Equation (17) against the non-dimensional distance from the wall $\eta = \alpha y$. The solid line represents the profile computed with the high-order scheme. One can see that the results obtained with the standard FD scheme (solid symbols) only on the finest grid $(N_x = N_y = N = 40)$ coincide with the HO scheme results.

4. RESULTS AND DISCUSSION

There are fundamental differences between a pulsating flow induced by low or high frequency pressure gradient oscillations. Using the asymptotic expansions of the expressions given by Equations (8) and (9), one obtains for a pulsating flow between two plates the following:

Slow oscillations, $\alpha h \ll 1$: $\phi_{U_m} \approx 0, \quad 12\mu\gamma_{U_m} L/\gamma_p h^2 \approx 1,$
$\phi_\tau \approx 0, \quad 2\gamma_\tau L/\gamma_p h \approx 1$

Fast oscillations, $\alpha h \gg 1$: $\phi_{U_m} \approx 90°, \quad 12\mu\gamma_{U_m} L/\gamma_p h^2 \approx 0,$
$\phi_\tau \approx 45°, \quad 2\gamma_\tau L/\gamma_p h \approx 0.$

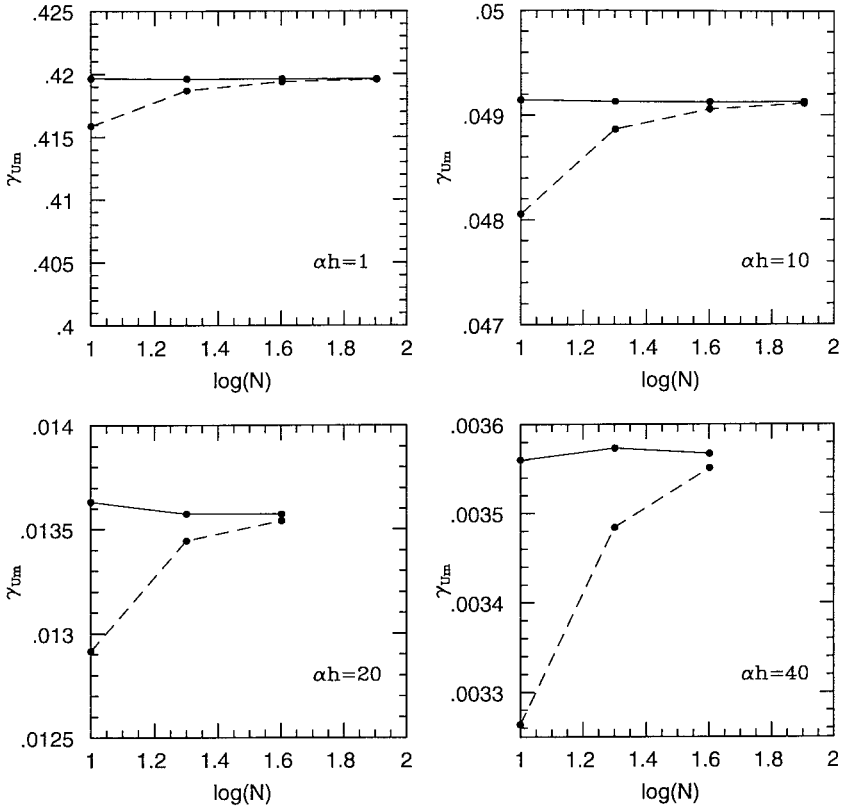

Figure 2. Mean velocity amplitude γ_{U_m}, for different meshes, $N_x = N_y = N$.

It follows for slow oscillations that there is no phase lag between the induced fluid motion and the imposed very slow pressure oscillations. In the fast oscillations case, the mean velocity and the wall shear stress oscillate with phase lags of 90° and 45° respectively, with respect to the imposed pressure oscillations.

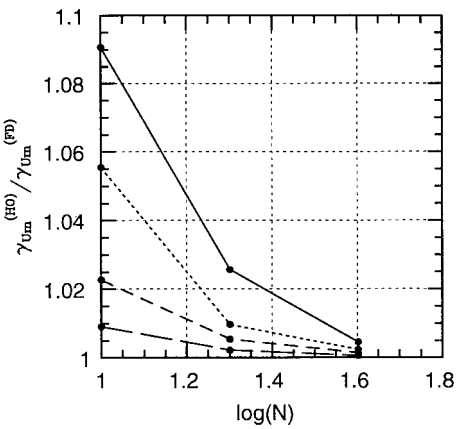

Figure 3. Ratio $\gamma_{U_m}^{(HO)}/\gamma_{U_m}^{(FD)}$ for different meshes, $N_x = N_y = N$.

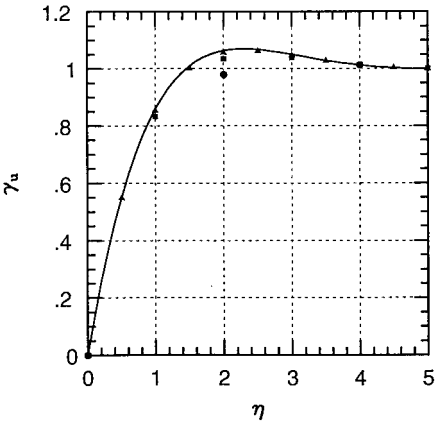

Figure 4. Amplitude γ_u of the induced velocity, $a/h = 1$, $\alpha h = 20$. Solid line: numerical results, high-order accuracy scheme, $N_x = N_y = 40$. Symbols: numerical results, second-order accuracy scheme; dots, $N_x = N_y = 10$; squares, $N_x = N_y = 20$; triangles, $N_x = N_y = 40$.

The motion of a viscous fluid in a duct caused by pressure gradient oscillations is characterized also by the depth of penetration of the viscous wave, $\delta = (2\nu/\omega)^{1/2}$. Two important limiting cases are possible depending on whether the quantity δ is large or small compared with a characteristic dimension of the duct. Let h, the distance between the walls in the y-direction, be chosen to be this characteristic dimension. The ratio h/δ is, for instance, the Reynolds number for the flow at hand. Introducing $\alpha = \delta^{-1} = (\omega/2\nu)^{1/2}$, the Reynolds number is defined as $\alpha h = (\omega/2\nu)^{1/2}h$. The first limiting case of low frequency oscillations ($\alpha h \ll 1$) means that the velocity varies very slowly with time, and the derivative term $\partial u/\partial t$ in the governing equation of motion can therefore, be neglected. Thus, the viscous term in the governing equation is balanced by the imposed pressure gradient term. Consequently, in this limiting case, the velocity varies periodically in the same phase as the pressure gradient. In the opposite case of high frequency oscillations, where the Reynolds number αh, is large, the viscous term can be neglected everywhere except in the very narrow layers near the walls. The width of these layers is of the order of magnitude of the depth of penetration of the viscous wave, $\delta \propto (\nu/\omega)^{1/2}$. This case is typical for boundary layers when, at a certain distance from the wall, the fluid moves as if it was frictionless. This implies that in this case ($\alpha h \gg 1$), the unsteady term $\partial u/\partial t$ in the governing equation is balanced (except in the narrow δ-layer) by the imposed oscillating pressure gradient term, i.e. the terms $\rho\, \partial u/\partial t$ and $-\partial p/\partial z$ are of the same order of magnitude. Therefore, at a large distance from the wall, the fluid is forced to move with a phase lag of 90° with respect to the exciting pressure gradient.

Calculations for low and high frequency regimes ($1 \leq \alpha h \leq 20$) in a rectangular duct with two different aspect ratios ($a/h = 1$ and 10) were performed. In the following, results appropriate to low ($\alpha h = 1$) and moderate ($\alpha h = 8$) frequencies will be presented and discussed. (Results for higher frequencies ($\alpha h \geq 10$) will not be presented, since, as will be shown subsequently (see Figure 13), their features are similar to those of the moderate frequency, i.e. $\alpha h = 8$.)

The results for a low frequency ($\alpha h = 1$) pulsating flow in a duct of square cross-sectional shape ($a/h = 1$) are presented in Figure 5. The variation of the pressure gradient with time for one period is shown in Figure 5(a). The velocity profiles at different time instants of one period and at different x-locations in the xy-cross-section of the duct are shown in Figure 5(b). For comparison, the velocity profiles for a one-dimensional flow between two parallel plates, as

calculated by Equation (4), are shown in Figure 5(c). Figure 5 indicates that the velocity distribution is in phase with the imposed pressure gradient. The induced velocity amplitude is seen to be smaller than that for the flow between two parallel plates (compare Figure 5(b) and (c)). This is due to the increase of the friction effects in the duct. The latter is clearly seen from the velocity profiles at x-locations close to the side wall: $x/a = 0.25$ (dashed line in Figure 5(b)) and $x/a = 0.1$ (dot-dashed line in Figure 5(b)).

For a rectangular duct with a high aspect ratio ($a/h = 10$), one may expect the velocity distributions to differ from those of the one-dimensional flow between two parallel plates only close to the side walls. The results of this case are shown in Figure 6. As shown in Figure 6(b), the velocity profiles at $x/a = 0.5$ (solid line) and $x/a = 0.1$ (dotted line) practically coincide with those between two parallel plates (compare with Figure 6(c)). As is evident in Figure 6(b), close to the side wall, at $x/a = 0.025$ (dashed line) and $x/a = 0.01$ (dot-dashed line), viscous effects become dominant and as a result the velocity amplitude decreases. From Figure 6, due to the relatively low frequency of the imposed pressure gradient ($\alpha h = 1$), the induced velocity is again seen to vary, practically in the same phase as the pressure.

Figures 7 and 8 show the results for a moderate frequency ($\alpha h = 8$) pulsating flow in ducts with two different cross-sectional shape ($a/h = 1$ and 10). First, the velocity distributions differ considerably from those obtained for the low frequency case (compare with Figures 5 and 6). Second, the phase of the induced velocity is shifted differently with respect to the exciting pressure in the regions close and far from the duct walls. Both these effects are in accordance with the remarks in the beginning of this section. The velocity profiles at different instants of one period at different x-locations in the xy-cross-section of the duct, with a square cross-section ($a/h = 1$), are shown in Figure 7(b). For comparison, in Figure 7(c), the velocity profiles for a one-dimensional flow between two parallel plates as calculated by Equation (4)

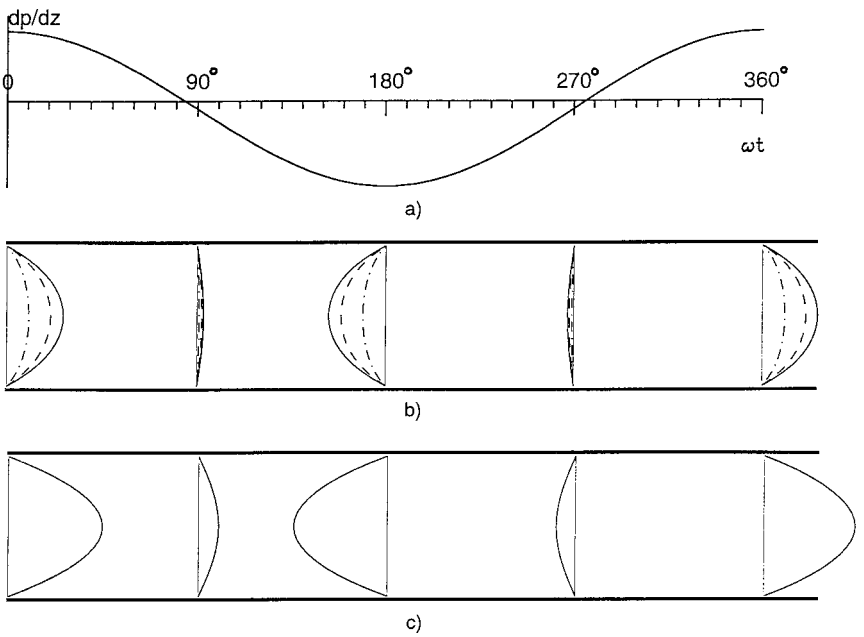

Figure 5. Velocity profiles in pulsating flow at different instants of one period. (a) Pressure gradient variation with time. (b) Duct flow, $a/h = 1$, $\alpha h = 1$: solid line, $x/a = 0.5$; dashed, $x/a = 0.25$; dot-dashed, $x/a = 0.1$. (c) Flow between two parallel plates.

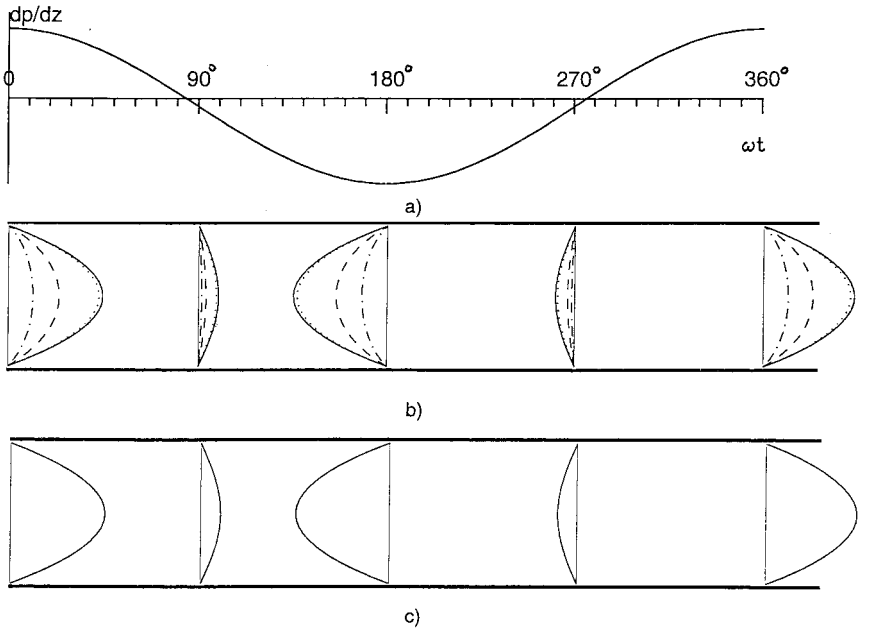

Figure 6. Velocity profiles in pulsating flow at different instants of one period. (a) Pressure gradient variation with time. (b) Duct flow, $a/h = 10$, $\alpha h = 1$: solid line, $x/a = 0.5$; dot, $x/a = 0.1$; dashed, $x/a = 0.025$; dot-dashed, $x/a = 0.01$. (c) Flow between two parallel plates.

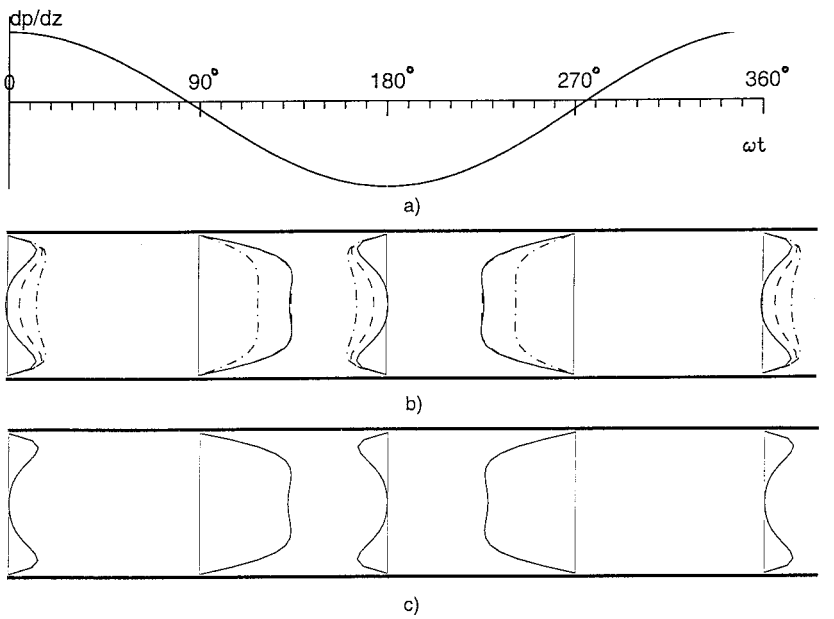

Figure 7. Velocity profiles in pulsating flow at different instants of one period. (a) Pressure gradient variation with time. (b) Duct flow, $a/h = 1$, $\alpha h = 8$: solid line, $x/a = 0.5$; dashed, $x/a = 0.25$; dot-dashed, $x/a = 0.1$. (c) Flow between two parallel plates.

are shown. Comparing the velocity distributions and the pressure variation with time yields that the flow at the duct axis (Figure 7(b), solid lines) lags behind that in the near-wall regions. At the axis, its phase is shifted by 90°, though this phase lag decreases when the side walls are approached (Figure 7(b), dashed and dot-dashed lines). The results indicate that at certain time instants, the velocity profiles have maximum values near the wall (Figures 7 and 8). This non-trivial effect, which is known as Richardson's 'annular effect', has been established experimentally [10] and analytically [11,12] for high frequency oscillating flows in a pipe. It implies that the time mean velocity squared has a maximum, which occurs near the pipe wall. (Recently, the authors have shown analytically [13] that Richardson's 'annular effect' also takes place for oscillating flows in ducts of arbitrary cross-sectional shapes.) It is interesting to note that at the middle section ($x/a = 0.5$, solid line in Figure 7(b)), the velocity profile (amplitude and phase) is practically the same as in the one-dimensional case (Figure 7(c)), though the duct has a square cross-section. As shown earlier, this is not the case for low frequency oscillations (Figure 5). This perhaps indicates, that for high-frequency oscillations, the viscous effects, being localized within a narrow near-wall region, are independent of the geometry of the duct. For a rectangular duct with a high aspect ratio ($a/h = 10$, Figure 8), the velocity distributions differ from those of the one-dimensional flow between two parallel plates only close to the side walls. The velocity profiles at $x/a = 0.5$ and 0.1 (solid lines in Figure 8(b)) completely coincide with those between two parallel plates (Figure 8(c)). Close to the wall, at $x/a = 0.025$ and 0.01 (dashed and dot-dashed lines respectively, in Figure 8(b)), viscous effects developing on the side wall are important and the flow becomes essentially two-dimensional.

The velocity variation with time at different points $(x, h/2)$ along the central $y = h/2$ plane (see Figure 1) for a low frequency ($\alpha h = 1$) pulsating flow in a duct of square cross-sectional shape ($a/h = 1$) is presented in Figure 9(b). The variation of the frictional force,

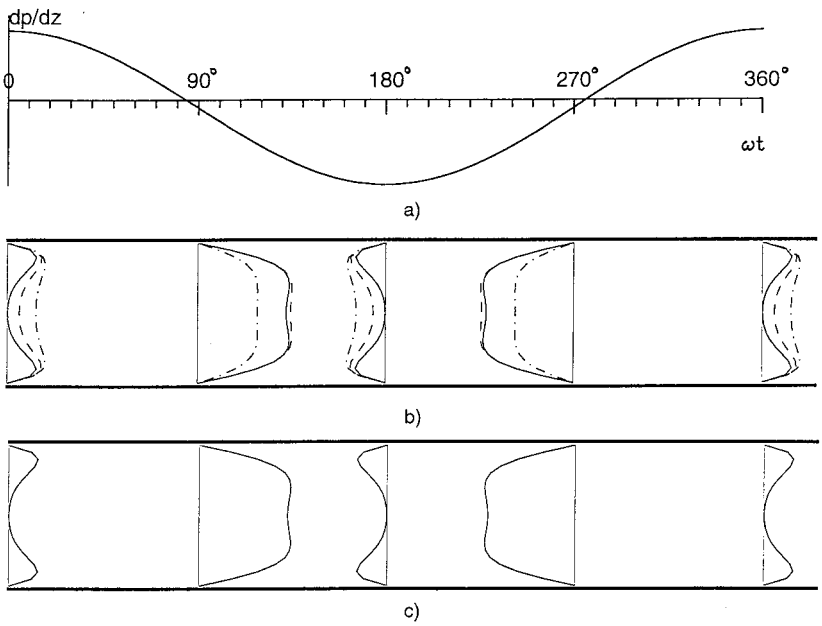

Figure 8. Velocity profiles in pulsating flow at different instants of one period. (a) Pressure gradient variation with time. (b) Duct flow, $a/h = 10$, $\alpha h = 8$: solid line, $x/a = 0.5$; dashed, $x/a = 0.025$; dot-dashed, $x/a = 0.01$. (c) Flow between two parallel plates.

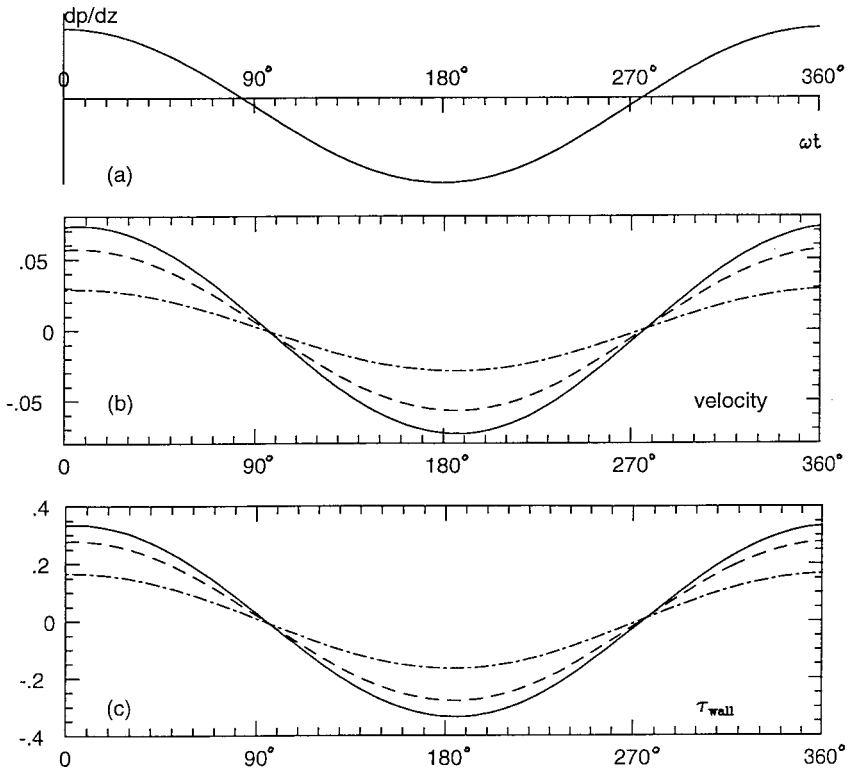

Figure 9. Pulsating duct flow, $a/h = 1$, $\alpha h = 1$. (a) Pressure gradient variation with time. (b) Velocity at $y/h = 0.5$: solid line, $x/a = 0.5$; dashed, $x/a = 0.25$; dot-dashed, $x/a = 0.1$. (c) Wall surface shear at $y = 0$: solid line, $x/a = 0.5$; dashed, $x/a = 0.25$; dot-dashed, $x/a = 0.1$.

$\tau_{\text{wall}} = \mu\, \partial u/\partial y|_{y=0}$, with time for one period at different x-locations at the wall is plotted in Figure 9(c). It is seen clearly that the velocity and the wall friction distributions are in phase with the imposed pressure gradient. The amplitude of the induced velocity and the wall frictional force decrease upon approaching the side wall (Figure 9(b) and (c), $x/a = 0.25$, dashed lines, and $x/a = 0.1$, dot-dashed lines). The latter is due to the flow approaching the duct corner, where the frictional force is zero.

For a low frequency ($\alpha h = 1$) pulsating flow in a rectangular duct with a high aspect ratio ($a/h = 10$), one may expect that the velocity and wall frictional force distributions differ from those at the center ($x/a = 0.5$, solid lines in Figure 10(b) and (c)) only close to the side walls. The results of this case are shown in Figure 10. As expected for a low frequency case, the velocity and the wall friction variations with time are practically in phase with the imposed pressure gradient. As seen in Figure 10, the variation with time of the velocity and the wall friction at $x/a = 0.5$ (solid line) and $x/a = 0.1$ (short-dashed line) practically coincide. Only close to the side wall, at $x/a = 0.025$ and 0.01 (dashed and dot-dashed lines respectively, Figure 10(a) and (b)), the variations with time of the velocity and the wall friction differ.

Figure 11(b) shows the velocity variation with time at different points $(x, h/2)$ along the central $y = h/2$ plane (see Figure 1) for a moderate frequency ($\alpha h = 8$) pulsating flow in a duct of square cross-sectional shape ($a/h = 1$). The variation of the frictional force with time for one period at different x-locations at the wall is plotted in Figure 11(c). It is seen that the phases

of the velocity and the wall friction variations at the center ($x/a = 0.5$, solid lines in Figure 11(b) and (c)) are shifted by 90° and 45° respectively, with respect to the imposed pressure gradient. Recall that the same 45° phase lag between the wall shear force and the imposed pressure oscillations with time occurs for the pulsating flow between two parallel plates. Note that the dashed lines in Figure 11(b) and (c) show the results computed at $x/a = 0.25$, which are very close to those at the center ($x/a = 0.5$, solid lines). This means that only very close to the side wall ($x/a = 0.1$, dot-dashed lines, Figure 11(b) and (c)) do the results differ from those obtained at the center.

For a duct with a high aspect ratio ($a/h = 10$), the velocity and the wall frictional force distributions differ from those at the center ($x/a = 0.5$) only close to the side walls. The results of this case are shown in Figure 12. The variations with time of the velocity and the wall friction at $x/a = 0.5$ and $= 0.025$ practically coincide. Only very close to the side wall, at $x/a = 0.01$ (dot-dashed lines in Figure 12(a) and (b)), do the variations with time of the velocity and the wall friction differ from those at $x/a = 0.5$.

The amplitude and the phase lag of the cross-sectional mean velocity, U_{m} (see Equation (8)), against αh are plotted in Figure 13. The phase lag, $\phi_{U_{\mathrm{m}}}$ with respect to the imposed frequency of the pressure oscillations is shown in Figure 13(a). It is seen that the results for the duct with a high aspect ratio ($a/h = 10$, dashed line) only slightly differ from those obtained for the one-dimensional flow between two parallel plates (solid lines). The cross-sectional mean

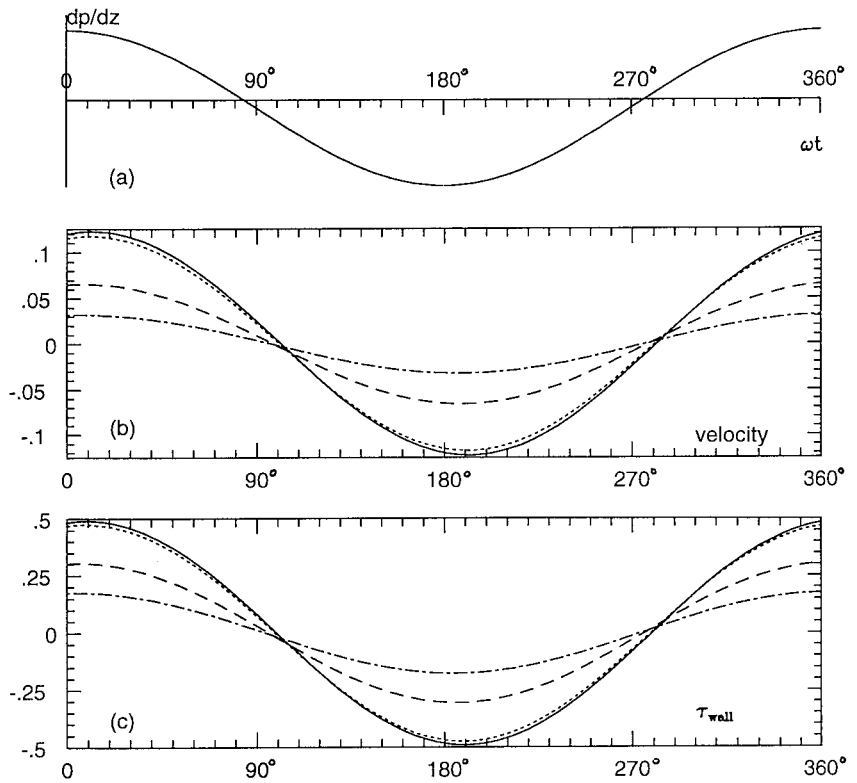

Figure 10. Pulsating duct flow, $a/h = 10$, $\alpha h = 1$. (a) Pressure gradient variation with time. (b) Velocity at $y/h = 0.5$: solid line, $x/a = 0.5$; dashed, $x/a = 0.025$; dot-dashed, $x/a = 0.01$. (c) Wall surface shear at $y = 0$: solid line, $x/a = 0.5$; dashed, $x/a = 0.025$; dot-dashed, $x/a = 0.01$.

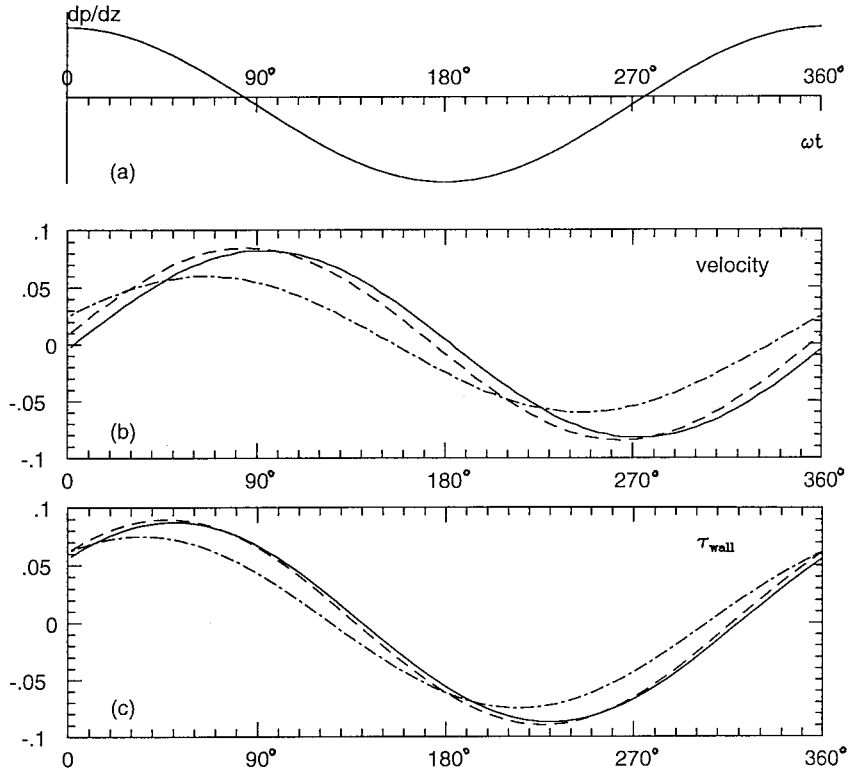

Figure 11. Pulsating duct flow, $a/h = 1$, $\alpha h = 8$. (a) Pressure gradient variation with time. (b) Velocity at $y/h = 0.5$: solid line, $x/a = 0.5$; dashed, $x/a = 0.25$; dot-dashed, $x/a = 0.1$. (c) Wall surface shear at $y = 0$: solid line, $x/a = 0.5$; dashed, $x/a = 0.25$; dot-dashed, $x/a = 0.1$.

velocity phase lag computed for a duct with a square cross-section ($a/h = 1$, dot-dashed line) is affected by two-dimensional effects and differs from that for the one-dimensional flow between two parallel plates. Recall that for the limiting case of $\alpha h \gg 1$, the phase lag $\phi_{U_m} \approx 90°$. The non-dimensional quantity β, which is the amplitude γ_{U_m} normalized by the amplitude of the imposed pressure oscillations, γ_p: $12\mu\gamma_{U_m}L/\gamma_p h^2$, is shown in Figure 13(b). As it follows from the calculations, the results for a square duct ($a/h = 1$, dot-dashed line) differ sufficiently from those obtained for the one-dimensional flow between two parallel plates (solid line), while $\alpha h < 6$. For a rectangular duct with a high aspect ratio ($a/h = 10$, dashed line), the results only differ slightly from the one-dimensional flow between two parallel plates (solid line) for already moderate imposed frequency of the pressure gradient oscillations, i.e. $\alpha h > 3$. The results indicate that the flow characteristics for a rectangular duct with a square cross-sectional shape ($a/h = 1$) are affected by two-dimensional effects.

In summary, the numerical results, as presented in this study, are in full agreement with the theoretical discussion in the beginning of this section regarding the physical differences between the flow response to imposed low and high frequency pressure difference oscillations.

5. CONCLUSIONS

A pulsating laminar flow of a viscous incompressible liquid in a rectangular duct was considered. The motion is induced by imposing a pulsating pressure difference. The problem was solved numerically. For the problem at hand, a high-order-accurate numerical scheme was used. The truncation error for the suggested scheme is of sixth-order $O(h^6)$ on a square mesh ($h_x = h_y = h$) and of fourth-order $O(h_x^4,\ h_x^2 h_y^2,\ h_y^4)$ on an unequally spaced mesh. Different flow regimes are characterized by a non-dimensional parameter based on the frequency of the imposed pressure gradient oscillations and the width of the duct. This is the Reynolds number of the problem at hand, which is defined as $\alpha h = (\omega/2\nu)^{1/2} h$.

Calculations for low and high frequency regimes ($1 \leq \alpha h \leq 20$) in a rectangular duct with different aspect ratios ($a/h = 1$ and 10) were performed. The induced velocity has a phase lag (shift) with respect to the imposed pressure oscillations, which varies from zero at very slow oscillations, to 90° at fast oscillations. The influences of the aspect ratio of the rectangular duct and the imposed pulsating pressure gradient frequency on the phase lag and the amplitude of the induced oscillating velocity and wall frictional force were analyzed.

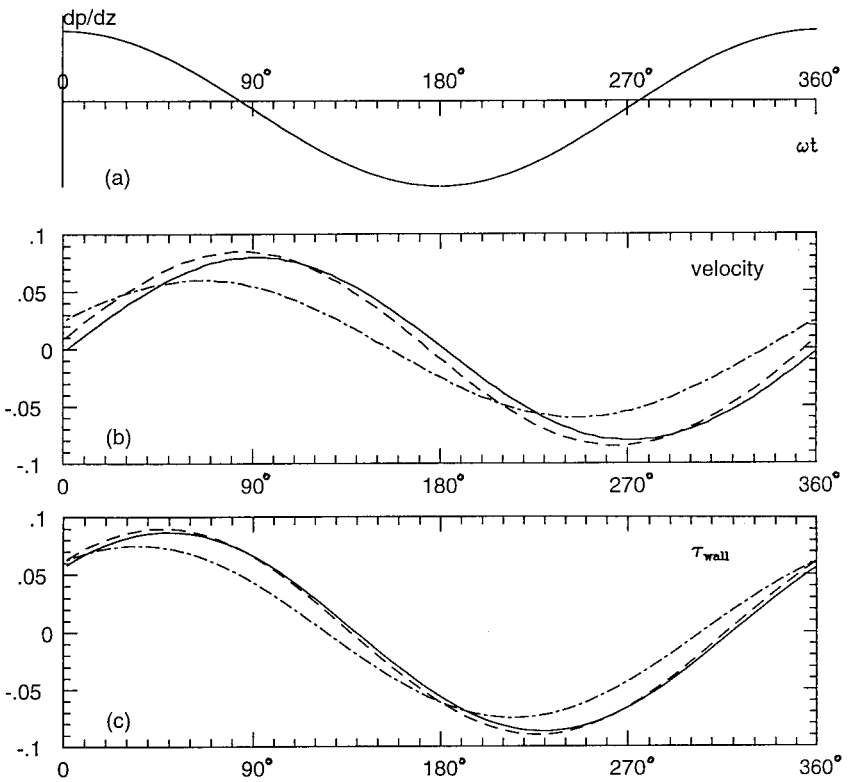

Figure 12. Pulsating duct flow, $a/h = 10$, $\alpha h = 8$. (a) Pressure gradient variation with time. (b) Velocity at $y/h = 0.5$: solid line, $x/a = 0.5$; dashed, $x/a = 0.025$; dot-dashed, $x/a = 0.01$. (c) Wall surface shear at $y = 0$: solid line, $x/a = 0.5$; dashed, $x/a = 0.025$; dot-dashed, $x/a = 0.01$.

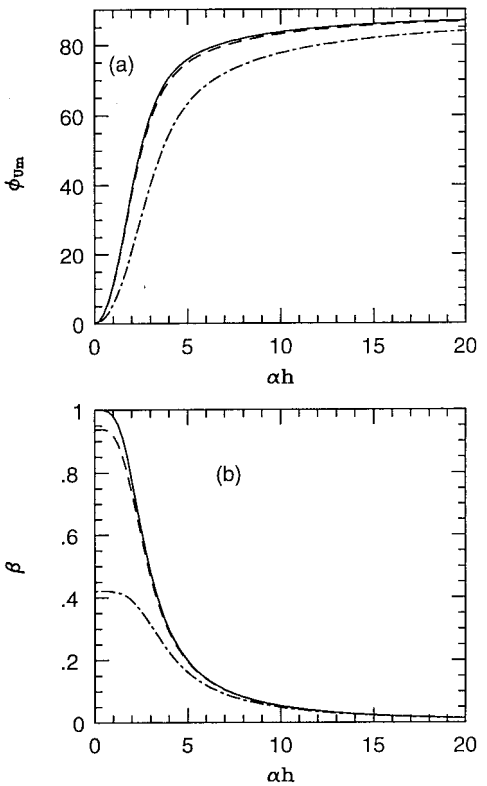

Figure 13. (a) Phase lag ϕ_{U_m}, and (b) amplitude $\beta = \gamma_{U_m}/(\gamma_p h^2/L\mu)$, of the cross-sectional mean velocity. Solid line, pulsating flow between two parallel plates; dashed, duct flow with $a/h = 10$; dot-dashed, duct flow with $a/h = 1$.

REFERENCES

1. H. Schlichting, *Boundary-Layer Theory*, McGraw-Hill, New York, 1979.
2. M. Arad, A. Yakhot and G. Ben-Dor, 'High-order-accurate discretization stencil for an elliptic equation', *Int. J. Numer Methods Fluids*, **23**, 367–377 (1996).
3. M. Arad, A. Yakhot and G. Ben-Dor, 'Highly accurate numerical solution of a biharmonic equation', *Numer. Methods Partial Differ. Equ.*, **13**, 375–391 (1997).
4. L.V. Kantorovich and V.I. Krylov, *Approximation Methods of Higher Analysis*, Wiley Interscience, New York, 1964.
5. D.M. Young and J.H. Dauwalder, 'Discrete representations of partial differential equations', in L.B. Rall (ed.), *Errors in Digital Computation*, Wiley, New York, 1965.
6. D.M. Young and R.T. Gregory, *A Survey of Numerical Mathematics*, vol. II, Addison-Wesley, Reading, MA, 1973.
7. R. Manohar and J.W. Stephenson, 'New high-order difference methods for solving the Poisson equation', *Congr. Numer.*, **34**, 483–493 (1982).
8. R. Manohar and J.W. Stephenson, 'Single cell high-order methods for Helmholtz equation', *J. Comput Phys.*, **51**, 448–453 (1983).
9. R. Manohar and J.W. Stephenson, 'High-order difference scheme for linear partial differential equations', *SIAM J. Sci. Stat. Comput.*, **5**, 69–77 (1984).
10. E.G. Richardson and E. Tyler, 'The transfer velocity gradient near the mouths of pipes in which an alternating or continuous flow of air is established', *Proc. Phys. Soc. Lond.*, **42**, 1–15 (1929).
11. T. Sexl, 'Uber den von E.G. Richardson entdeckten annulareffekt', *Z. Phys.*, **61**, 349 (1930).
12. C. Uchida, 'The pulsating viscous flow superposed on the steady motion of incompressible fluid in a circular pipe', *ZAMP*, **7**, 403–421 (1956).
13. A. Yakhot, M. Arad and G. Ben-Dor, 'Richardson's annular effect in oscillating laminar duct flows', *J. Fluids Eng.*, **120**, 209–211 (1998).

